JOURNAL OF SOLID STATE CHEMISTRY **124,** 1–7 (1996)
ARTICLE NO. 0199

A Mercury-Based Ferrite with a 0201–1201 Structure: (Hg, Pr)$Sr_4Fe_2O_9$

Ph. Boullay, B. Domengès, D. Groult, and B. Raveau

Laboratoire CRISMAT-ISMRA, Bd Maréchal Juin, 14050 Caen Cedex, France

Received September 18, 1995; in revised form January 19, 1996; accepted January 23, 1996

The mercury-based ferrite (Hg, Pr)$Sr_4Fe_2O_9$ is studied by XRPD and HREM. The $Hg_{0.3}Pr_{0.6}Sr_4Fe_2O_9$ structure is confirmed as of "0201–1201" type and it is shown that the ordering of Hg-Pr and its oxygen neighboring framework takes place. © 1996 Academic Press, Inc.

INTRODUCTION

Numerous mercury based superconducting cuprates have been synthesized after the discovery of $HgBa_2CuO_{4+\delta}$ (1). Most of them require the presence of a foreign element on the mercury site to be stabilized. This is especially the case of the "Hg–Sr" cuprates which can only be obtained by introducing either lead or bismuth or a lanthanide or a transition element on the Hg sites leading to the generic formula (Hg, $M)_1Sr_2$(Ca, $Ln)_{n-1}Cu_nO_{2n+2+\delta}$ (2–9). Though the structural principles that govern these phases are established, the nature of the [(Hg, $M)_1O_{1-\delta}$] layers and their role in the superconductivity phenomenon are so far not understood. Curiously, no ordering between M and Hg is evidenced in most of these layers in spite of the different coordination generally observed for Hg and M. Among the various substituted mercury layers, only one kind, involving praseodymium, was found to exhibit a cationic ordering between Hg and Pr (10). One important issue is to determine whether such mixed layers are specific of cuprates or if they can be extended to other transition metal nonsuperconducting oxides that do not exhibit the Jahn–Teller effect. For this reason we have investigated the system Hg–Pr–Sr–Fe–O. We report herein on a new ferrite, (Hg, Pr)$Sr_4Fe_2O_9$, which corresponds to an intergrowth of the **0201** (La_2CuO_4-type) and **1201** ($HgBa_2CuO_4$-type) structures and exhibits like the Hg–Pr cuprates a cationic ordering in the mercury layers.

EXPERIMENTAL

Synthesis

(Hg, Pr)$Sr_4Fe_2O_9$ compounds were prepared in a two step procedure: first, appropriate mixtures of Fe_2O_3, $SrCO_3$, and Pr_6O_{11} were intimately ground in an agate mortar and heated in air at 950°C for 1 day. Second, after adding the adequate HgO amount, mixtures were packed in an alumina finger and heated in an evacuated silica tube. A lot of different thermal treatments, several cation ratios, and several oxygen contents (using SrO precursor) were tried and the best results were obtained for the $Hg_{0.4}Pr_{0.6}Sr_4Fe_2O_9$ starting composition and samples introduced at 400°C, heated up to 880°C for 8 h, and then cooled down with furnace inertia. Obtained powders are dark colored and appeared stable in air.

Powder X-Ray Diffraction Study

A primary powder X-ray diffraction analysis, performed with a Guinier camera, allowed a new phase isotypic to the **0201–1201** intergrowth ($Pb_{1-x}Tl_x$)$Sr_4Fe_2O_9$ (11) to be synthesized. Nevertheless, the formation of small amounts of a secondary phase derived from the Sr–Fe–O system, of $Sr_3Fe_2O_7$-type, could never be avoided. The powder X-ray diffraction patterns were registered on a Philips diffractometer using the Cu$K\alpha$ radiation, equipped with a graphite back-scattering monochromator, from 5° to 120° (2θ) in 0.02° steps. The data were refined with the program FULLPROF (12).

Electron Microscopy Study

Powders were gently ground in an agate mortar in *n*-butanol and deposited on a holey carbon coated copper grid. Electron diffraction (ED) was performed on a JEM200CX equipped with a tilting rotating goniometer (±60°), which allows the reciprocal space reconstruction, and the high resolution study was performed on a TOP-

0022-4596/96 $18.00

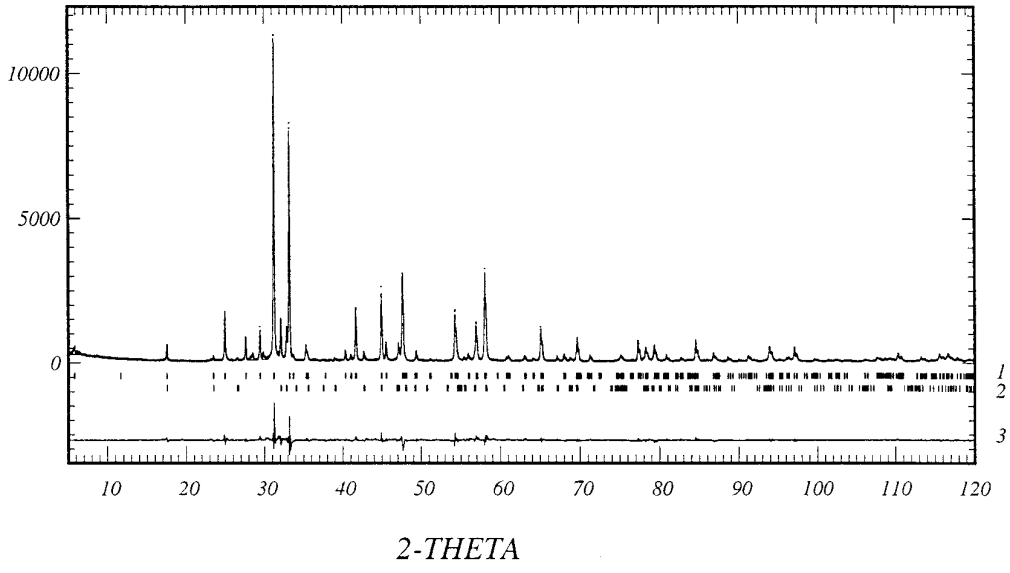

FIG. 1. X-ray powder diffraction pattern of $Hg_{0.3}Pr_{0.6}Sr_4Fe_2O_9$ compound. (1) $Hg_{0.3}Pr_{0.6}Sr_4Fe_2O_9$ reflections; (2) $(Sr, Pr)_3Fe_2O_7$ reflections; (3) difference pattern.

CON 2B electron microscope equipped with a ±10° double tilt goniometer and an objective lens with spherical aberration constant of 0.4 mm. High resolution images (HREM) were simulated using the multislice method of EMS package. Both microscopes are equipped with KEVEX EDS analyzers, which allowed the determination of the precise composition of the **0201–1201** intergrowth-type phase, and thus the observed Hg/Pr ratio is most often close to 0.5.

$Hg_{0.4}Pr_{0.6}Sr_4Fe_2O_9$ STRUCTURAL STUDY

At a first sight, the indexation of the powder X-ray diffraction pattern (Fig. 1) and the ED observations confirm the tetragonal symmetry, with reflection existence conditions $h\ k\ l/h + k + l = 2n$, and the XRPD pattern is indexed in a tetragonal cell with $a = 3.8156(1)$ Å, $c = 30.3385(5)$ Å. Nevertheless, a careful study of the [001] ED patterns also suggests that a slight deviation from te-

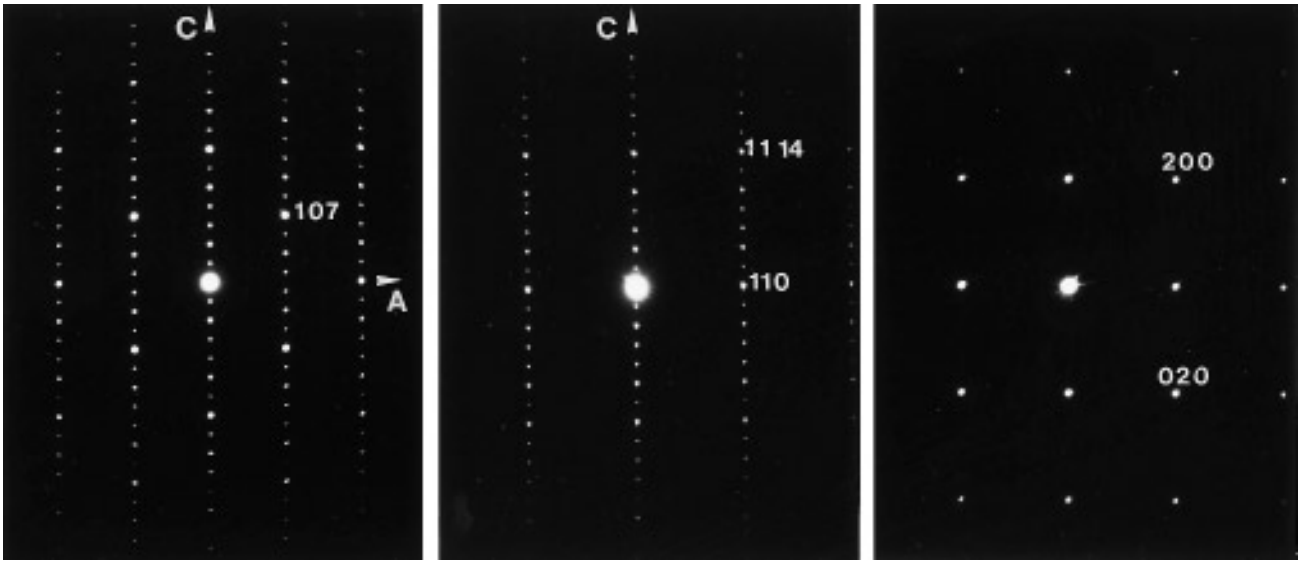

FIG. 2. [010], [$1\bar{1}0$], and [001] ED patterns showing reflection conditions $h0l$: $h + l = 2n$, hhl: $l = 2n$, $hk0$: $h + k = 2n$ compatible with *Immm* space group.

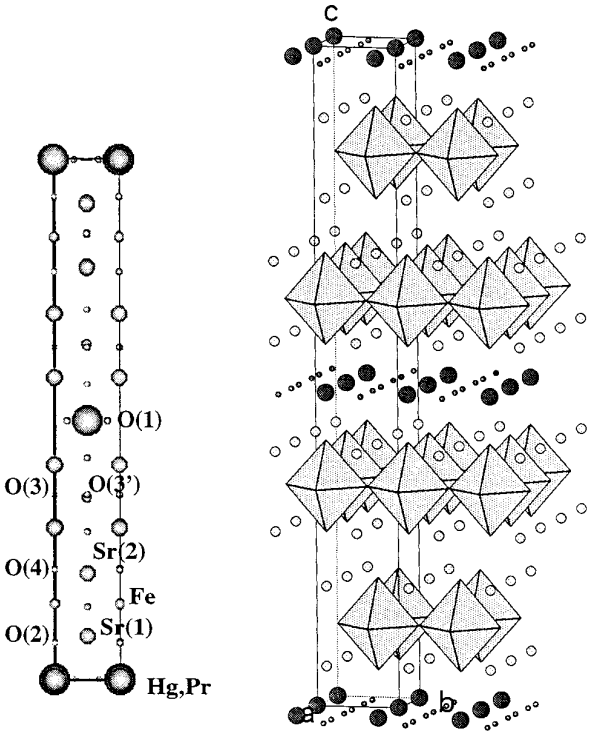

FIG. 3. (Hg, Pr)$Sr_4Fe_2O_9$ structure: (a) schematic [010] projection, (b) perspective view.

tragonality $a \cong b$ takes place (Fig. 2). This could be related to an ordering phenomenon which was characterized through the frequent existence on ED patterns of diffuse streaks parallel to the reciprocal *C* parameter involving a doubling of the *a* parameter. Indeed, the reconstruction of the reciprocal space shows that only the *a* parameter is doubled and not *b* which leads to the orthorhombicity of the subcell $a_p \times a_p \times c$. HREM observations allow us to precisely determine this ordering phenomenon, that we will discuss below.

The refinement of the structure is performed, based on **0201–1201** ideal structural parameters but in the orthorhombic *I mmm* space group: the considered stacking sequence is thus [(Hg, Pr)O_δ–SrO–FeO_2–SrO–SrO–FeO_2–SrO] (Fig. 3a). The secondary $Sr_3Fe_2O_7$-type phase was introduced in the refinement and treated in a pattern matching mode. Its refined parameters $a = 3.8554(4)$ Å (*I* 4/*mmm* space group), slightly different from those of

TABLE 1
$(Hg_{0.3}Pr_{0.57})Sr_4Fe_2O_9$ Structural Parameters

Atom	Site	*x*	*y*	*z*	B(Å^2)	Occupancy
Hg	2*a*	0	0	0	0.8(1)	0.30(1)
Pr	2*a*	0	0	0	0.8(1)	0.57(1)
Sr(1)	4*i*	0.5	0.5	0.0839(2)	0.8(1)	1[a]
Sr(2)	4*i*	0.5	0.5	0.2054(2)	0.7(1)	1[a]
Fe	4*i*	0	0	0.1476(3)	1.2(2)	1[a]
O(1)	2*c*	0.19[b]	0	0.5	1[c]	0.5
O(2)	4*i*	0	0	0.071(1)	1[c]	1
O(3)	4*j*	0.5	0	0.1412(8)	1[c]	1
O(3′)	4*j*	0	0.5	0.1412(8)	1[c]	1
O(4)	4*i*	0	0	0.214(1)	1[c]	1

Note. Space group *I mmm*; $z = 2$; $a = 3.8174(2)$ Å, $b = 3.8138(2)$ Å, $c = 30.339(1)$ Å. $R_p = 9.1\%$, $R_{wp} = 12.0\%$, $R_{exp} = 7.1\%$, $\chi^2 = 2.9$, and $R_I = 5.9\%$.

[a] Site occupancies were refined to be full and then fixed.

[b] Split $x_{O(1)}$ position was deduced in parallel from HREM study and manually refined, leading to the best *R* values and correct interatomic distances.

[c] The isotropic thermal parameter values of oxygen atoms were fixed to 1 Å^2.

TABLE 2
$(Hg_{0.3}Pr_{0.57})Sr_4Fe_2O_9$ Interatomic Distances (Å)

Hg, Pr	–O(1)	4×2.24 or 4×3.25
	–O(2)	2×2.16
Sr (1)	–O(1)	2×2.65
	–O(2)	4×2.73
	–O(3)	2×2.58
	–O(3′)	2×2.58
Sr(2)	–O(3)	2×2.73
	–O(3′)	2×2.73
	–O(4)	$4 \times 2.71 + 1 \times 2.45$
Fe	–O(2)	1×2.32
	–O(3)	2×1.92
	–O(3′)	2×1.92
	–O(4)	1×2.01

Note. Standard deviations on interatomic distances are close to 0.02 Å.

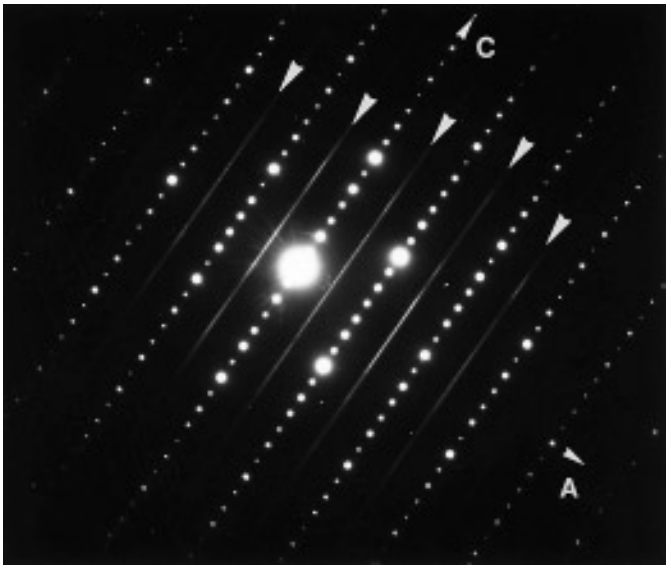

FIG. 4. Characteristic [010] ED pattern showing diffuse streaks parallel to *C* which involve a doubling of *a* parameter.

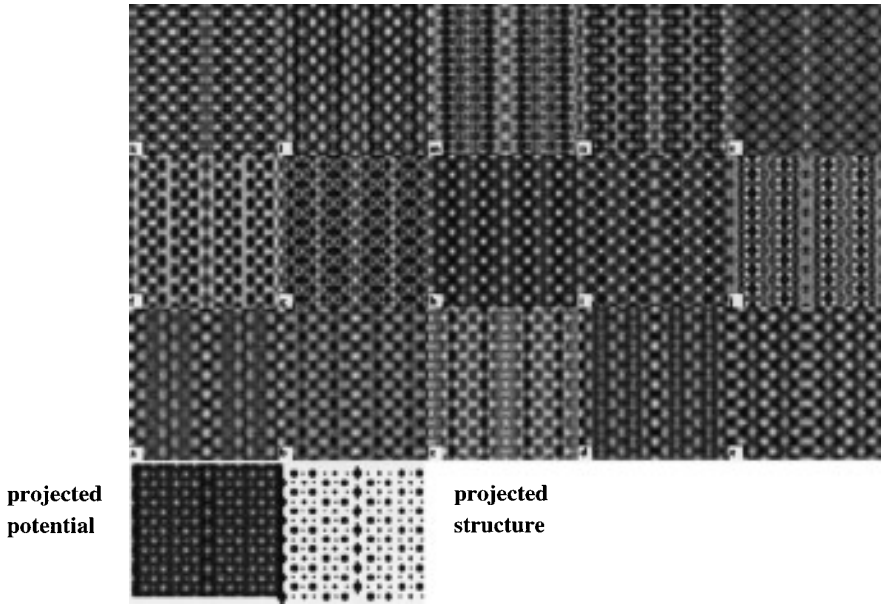

FIG. 5. $Hg_{0.3}Pr_{0.6}Sr_4Fe_2O_9$. Calculated through focus series with following parameters: high voltage $V = 200$ kV, crystal thickness $t = 3.4$ nm, Cs = 0.4 mm, objective aperture radius $R = 20$ nm^{-1}, spread of focus $\Delta = 10$ nm, beam half-convergence $\alpha = 0.85$ mrad, focus ranging from (a) 20 to (o) − 120 nm by 10 nm steps.

$Sr_3Fe_2O_{7-\delta}$ phases (13), suggest the substitution of praseodymium for strontium in agreement with EDS observations which lead to the mean composition $Sr_{2.8}Pr_{0.2}Fe_2O_{7\pm\delta}$.

Structure refinement confirms the **0201–1201** structural type of the $Hg_{0.4}Pr_{0.6}Sr_4Fe_2O_9$ compound (Table 1) and two main results can be pointed out:

(i) The Hg site is partly occupied by praseodymium, but it is also cation deficient, leading to the $[Hg_{0.3}Pr_{0.6}\square_{0.1}O_\delta]$ layer composition.

(ii) As suggested by the HREM study the mean $Hg_{0.3}Pr_{0.6}Sr_4Fe_2O_9$ structure is resolved with the O(1) split on two different positions, which ensures then two different environments for the mixed (Hg, Pr) site.

Thus, the $Hg_{0.3}Pr_{0.6}Sr_4Fe_2O_9$ structure (Fig. 3b) can be described as the regular intergrowth of the Sr_2FeO_4 structure (**0201**) with the cation deficient $Hg_{0.3}Pr_{0.6}Sr_2FeO_5$ (**1201**) structure. Although the X-ray powder diffraction study does not allow us to determine accurately the oxygen atom positions in the structure, it can be noticed that the interatomic distances are close to those observed for these kind of oxides (Table 2) and follow the same evolution as in the other **0201–1201** type structures. The FeO_6 octahedra are elongated along *c*, the iron cation being off centered toward the SrO–SrO layers so that it exhibits an almost pyramidal environment. In the rock salt-type layer, one can distinguish two environments: an almost regular octahedral coordination which would correspond to a praseodymium rich (Hg, Pr) site and an almost twofold coordination more suitable for a mercury rich site.

The electron transmission electron microscopy study allows us to characterize the microstructure of these compounds. Besides the evidence of good cristallinity of the samples and the great regularity in layer stacking, a lot of slightly rotated domains were detected through the presence of split dots forming arcs on ED patterns. However, as presented above, the more important observation deals with the frequent existence on ED patterns of diffuse streaks parallel to the reciprocal *C* parameter which imply a doubling of the *a* parameter (Fig. 4). This phenomenon can be interpreted as an ordering phenomenon along *a* but which does not occur regularly along the *c* direction, in a similar way to that observed in the **1222**-type cuprate $Hg_{0.4}Pr_{0.6}Sr_2(Pr_{1.7}Sr_{0.3})Cu_2O_{8\pm\delta}$ (10). Thus, it appeared necessary to investigate the $Hg_{0.3}Pr_{0.6}Sr_4Fe_2O_9$ compound by high resolution electron microscopy; the [010] observation direction was chosen as most representative of the structure and the ordering phenomenon. In order to interpret the observed contrast, high resolution images were calculated based on the structural results of the X-ray powder diffraction study. Figure 5 shows a calculated through focus series for a crystal thickness of 3.4 nm. Three characteristic images are described, which were observed (Fig. 6). For the 10 nm focus value, high electron density zones are highlighted and the mixed (Hg, Pr) sites appear as very bright dots, whereas the Sr sites are slightly less highlighted and the FeO rows correspond to the grey dots. For the −30 nm focus value, low electron density zones of the structure

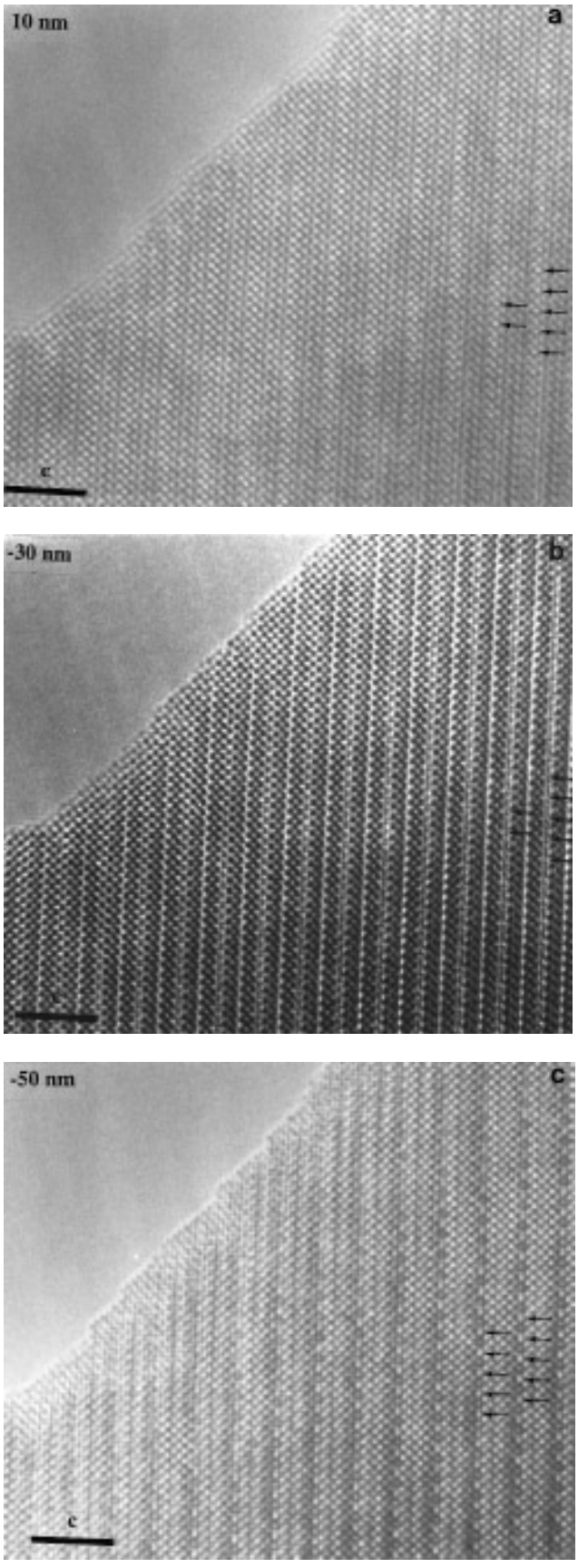

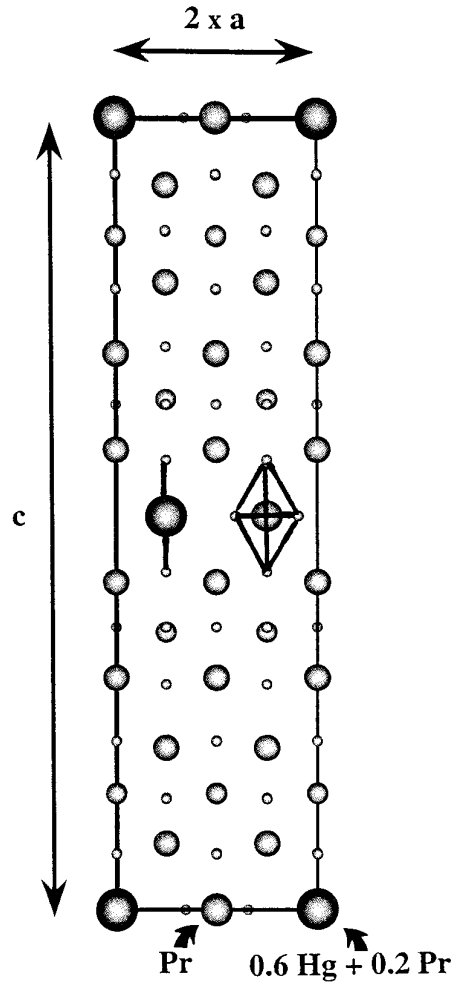

FIG. 7. [010] projection of a model involving an ordering along the *a* direction of the Hg and Pr cations and the displacement of neighboring oxygen O(1).

are highlighted and the oxygen atoms appear as bright dots, the partially occupied oxygen sites of the (Hg, Pr)O_δ layer appear as large splitted bright dots, and Sr and Fe sites appear as very dark dots. For the −50 nm focus value, again high electron density zones of the structure are highlighted and the cationic sites appear as bright dots, but for that focus value, the Fe sites appear as the brightest. The observed contrasts are in good agreement with those calculated (Fig. 5) but as the thickness increases a modulation of contrast related to the doubling of the *a* parameter is observed, especially for the −50 nm image. This can be described, for an intermediate thickness, as

FIG. 6. Three focus value [010] experimental images (10, −30, and −50 nm) corresponding to the ED pattern of Fig. 4. Modulation of contrast is observed on thicker area of the crystal (arrowed).

the regular succession along *a* of one grey dot and one brighter dot that takes place at the level of the (Hg, Pr)O_δ layer; considering the focus value, this suggests that the contrast modulation is related to the ordering of the Hg–Pr cations. Further image calculations have been performed trying to determine this ordering phenomenon. It appeared that the only ordering of Hg and Pr cations with a unique O(1) site is not sufficient to explain modulation of the contrast, even for thicknesses as high as 16 nm. We have indeed to consider the fact that Hg and Pr cations should not have the same environment; thus a model can be proposed, based on a displacement of oxygen atoms of the layer which corresponds for praseodymium to an almost regular octahedral coordination, with four short Pr–O equatorial distances of about 2.25 Å, and for mercury to a 2 + 4 coordination, with four equatorial distances of 3.25 Å, compatible with its twofold coordination (Fig. 7). In relation to the resolved mean structure, the composition of our model was kept as $Hg_{0.3}Pr_{0.6}Sr_4Fe_2O_9$, with a mixed $[Hg_{0.6}Pr_{0.2}]_\infty$ row alternating with a $[Pr_1]_\infty$ one along *a*. Based on such a model, the calculated images show a modulation of the contrast for thicknesses as low as 2.3 nm depending on the focus value (Fig. 8). The comparison of the observed image of Fig. 6c with that calculated for a −50 nm focus value and 5.7 nm thickness gives a good agreement. It confirms that the ordering phenomenon indeed involves the Hg and Pr cations but also the oxygen atoms that surround these cations in the $[(Hg, Pr)O]_\infty$ layer. The rather large distance between two successive $[(Hg, Pr)O]_\infty$ layers (1.5 nm) does not allow us to stabilize the Hg–Pr ordering in a correlated way so that no superstructure is observed along *c*, but only diffuse streaks parallel to *C*. An elemental monoclinic unit can be defined and the whole observed matrix can be easily described by successive chemical twinnings parallel to the (001) plane (Fig. 9).

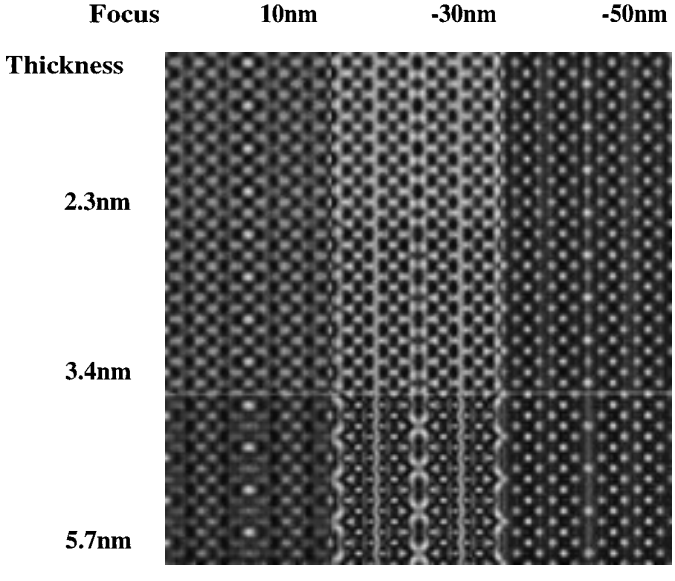

FIG. 8. Three characteristic images of the through focus series calculated with the structural parameters of the previous model for different thicknesses of the crystal ($Hg_{0.3}Pr_{0.6}Sr_4Fe_2O_9$, ordered model).

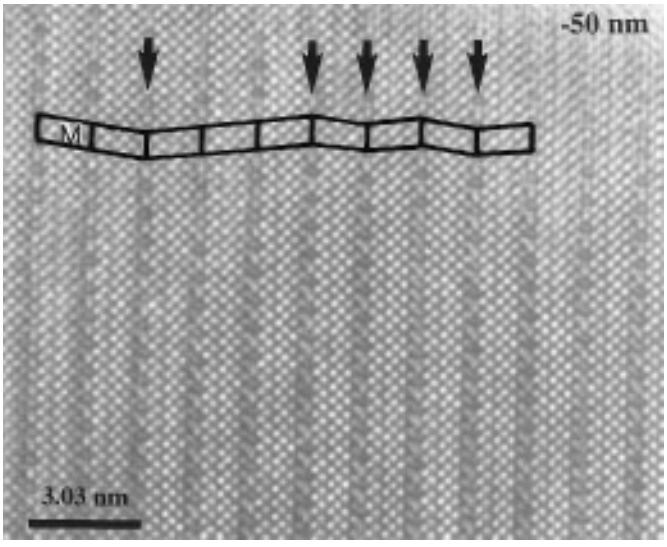

FIG. 9. Thicker area of the crystal shown on experimental images of Fig. 6, −50 nm focus value. The elemental monoclinic cell is drawn (M) and several chemical twinnings (arrowed) are observed.

CONCLUSION

This study has shown that a regular **0201–1201** intergrowth structure can be stabilized in the Hg–Pr–Sr–Fe–O system. In a similar way to the related cuprates, the obtained phase stabilized with the $Hg_{0.3}Pr_{0.6}Sr_4Fe_2O_9$ composition is characterized by ordering phenomena. It is also shown here that the latter do not only involve the Hg–Pr cations but also the oxygen neighboring framework.

REFERENCES

1. S. N. Putilin, E. V. Antipov, O. Chmaissen, and M. Marezio, *Nature* **362,** 226 (1993).
2. D. Pelloquin, C. Michel, G. Van Tendeloo, A. Maignan, M. Hervieu, and B. Raveau, *Physica C* **214,** 87 (1993).
3. A. Maignan, C. Michel, G. Van Tendeloo, M. Hervieu, and B. Raveau, *Physica C* **216,** 1 (1993).
4. F. Goutenoire, Ph. Daniel, M. Hervieu, G. Van Tendeloo, C. Michel, A. Maignan, and B. Raveau, *Physica C* **216,** 243 (1993).
5. D. Pelloquin, M. Hervieu, C. Michel, G. Van Tendeloo, A. Maignan, and B. Raveau, *Physica C* **216,** 257 (1993).
6. M. Hervieu, G. Van Tendeloo, A. Maignan, C. Michel, F. Goutenoire, and B. Raveau, *Physica C* **216,** 264 (1993).

7. C. Martin, M. Hervieu, M. Huve, C. Michel, A. Maignan, G. Van Tendeloo, and B. Raveau, *Physica C* **222,** 19 (1994).
8. J. Shimoyama, S. Hahakura, K. Kitazawa, K. Yamafuji, and K. Kishio, *Physica C* **224,** 1 (1994).
9. S. Hahakura, J. Shimoyama, O. Shiino, and K. Kishio, *Physica C* **223,** 1 (1994).
10. G. Van Tendeloo, M. Hervieu, X. F. Zhang, and B. Raveau, *J. Solid State Chem.* **114,** 369 (1995).
11. Ph. Daniel, L. Barbey, D. Groult, N. Nguyen, G. Van Tendeloo, and B. Raveau, *Eur. J. Solid State Inorg. Chem.* **31,** 235 (1994).
12. J. Rodriguez-Carjaval, "Proc. Satellite Meeting on Powder Diffraction of the XVth Congress of Int. Union of Crystallography." Toulouse, France, July 1990.
13. S. E. Dann, M. T. Weller, and D. B. Currie, *J. Solid State Chem.* **97,** 179 (1992).